ADVANCES IN ATMOSPHERIC SCIENCES, VOL. 34, SEPTEMBER 2017, 1047–1056

• **Original Paper** •

Simulated Sensitivity of the Tropical Cyclone Eyewall Replacement Cycle to the Ambient Temperature Profile

Xulin MA, Jie HE, and Xuyang GE*

Collaborative Innovation Center on Forecast and Evaluation of Meteorological Disasters, Key Laboratory of Meteorological Disaster, Nanjing University of Information Science and Technology, Nanjing 210044*, China*

(Received 8 December 2016; revised 27 March 2017; accepted 5 April 2017)

ABSTRACT

In this study, the impacts of the environmental temperature profile on the tropical cyclone eyewall replacement cycle are examined using idealized numerical simulations. It is found that the environmental thermal condition can greatly affect the formation and structure of a secondary eyewall and the intensity change during the eyewall replacement cycle. Simulation with a warmer thermal profile produces a larger moat and a prolonged eyewall replacement cycle. It is revealed that the enhanced static stability greatly suppresses convection, and thus causes slow secondary eyewall formation. The possible processes influencing the decay of inner eyewall convection are investigated. It is revealed that the demise of the inner eyewall is related to a choking effect associated with outer eyewall convection, the radial distribution of moist entropy fluxes within the moat region, the enhanced static stability in the inner-core region, and the interaction between the inner and outer eyewalls due to the barotropic instability. This study motivates further research into how environmental conditions influence tropical cyclone dynamics and thermodynamics.

Key words: tropical cyclone, eyewall replacement cycle, ambient temperature profile

Citation: Ma, X. L., J. He, and X. Y. Ge, 2017: Simulated sensitivity of the tropical cyclone eyewall replacement cycle to the ambient temperature profile. *Adv. Atmos. Sci.*, **34**(9), 1047–1056, doi: 10.1007/s00376-017-6302-4.

1. Introduction

Intense tropical cyclones (TCs) frequently have a secondary eyewall (Willoughby et al., 1982; Black and Willoughby, 1992; Hawkins et al., 2006; Kuo et al., 2008). During the eyewall replacement cycle (ERC), TCs can experience striking changes in both intensity and structure. The mechanisms of secondary eyewall formation (SEF) have been extensively studied (Willoughby et al., 1982; Nong and Emanuel, 2003; Kuo et al., 2004, 2008; Terwey and Montgomery, 2008; Judt and Chen, 2010; Qiu et al., 2010; Zhou and Wang, 2011; Bell et al., 2012; Huang et al., 2012; Rozoff et al., 2012; Abarca and Montgomery, 2013; Qiu and Tan, 2013; Zhu and Zhu, 2014, 2015; Zhu et al., 2015; Zhang et al., 2017), but there is not yet a consensus on the underlying physics for SEF. It is hypothesized that both internal dynamics and external forcing play important roles in SEF. Nong and Emanuel (2003) suggested that SEF is likely triggered by external forcing, such as an upper-tropospheric baroclinic eddy. Montgomery and Kallenbach (1997) emphasized the role of inner-core dynamics, such as vortex Rossby waves (VRWs). It was proposed that the outer eyewall emanates at the stagnation radius of outward-propagating VRWs, as they accelerate the mean tangential flow through eddy momentum flux convergence. Terwey and Montgomery (2008) suggested that a "β-skirt" is required for the formation of a secondary eyewall. More recently, numerous studies (e.g., Huang et al., 2012; Abarca and Montgomery, 2013) have focused on the idea of unbalanced boundary layer dynamics; specifically, a broadening of the tangential wind, with enhanced supergradient winds in the boundary layer, forces convection outside the primary eyewall, leading to SEF. Qiu and Tan (2013) also emphasized that an unbalanced boundary layer responding to asymmetric inflow forcing induced by outer rainbands triggers the sustained convection outside the primary eyewall during the early phase of SEF.

While many studies have focused on the triggering mechanism for SEF, there have been comparatively fewer studies that have examined the structure of the secondary eyewall and the associated changes in intensity during an ERC (Yang et al., 2013; Zhou and Wang, 2013). Based on the different evolutionary features of secondary eyewalls, Yang et al. (2013) categorized typhoons into three groups: TCs that undergo an ERC; a concentric eyewall structure with no ERC; and a concentric eyewall structure that sustains for an extended period. For TCs with different concentric eyewall types, the intensity fluctuation shows great variability. For instance, some

* Corresponding author: Xuyang GE
Email: xuyang@nuist.edu.cn

© Institute of Atmospheric Physics/Chinese Academy of Scences, and Science Press and Springer-Verlag Berlin Heidelberg 2017

TCs with a concentric eyewall may maintain their intensity or even intensify during the ERC, which is different from the widely-held viewpoint that TCs would experience significant weakening (Willoughby et al., 1982; Houze et al., 2007). The structure of the secondary eyewall also shows great variability (Zhou and Wang, 2013), as the moat area varies from 10 to more than 100 km in diameter. Moreover, it is found that a TC with a larger secondary eyewall generally experiences more weakening. In practice, the structural change is an important issue for operational forecasting, since the ERC leads to a broadening of the damaging wind, which affects the extent of the damaging wind, storm surge and heavy rainfall. The structure of the secondary eyewall is associated with TC inner-core dynamics and thermodynamics (Rozoff et al., 2006; Houze et al., 2007; Zhou and Wang, 2011). The large-scale environmental conditions likely influence SEF (Kossin and Sitkowski, 2009; Zhou and Wang, 2013; Ge, 2015). For instance, the observational study of Zhou and Wang (2013) and the numerical study of Ge (2015) revealed that a TC will tend to generate a secondary eyewall at a wider radius in a moist environment. This motivates us to further explore the environmental impacts on SEF and the structure and intensity change during an ERC.

The rest of this paper is organized as follows: The model configuration and idealized experimental design are introduced in section 2. Section 3 compares the overall characteristics of the simulated secondary eyewall under different environmental thermal conditions. Section 4 analyzes the possible mechanisms accounting for different ERC characteristics. Finally, a short conclusion and discussion comprise section 5.

2. Model and experimental design

The simulations are performed using version 3.3.1 of the Advanced Research version of the Weather Research and Forecasting model (WRF-ARW). The model simulations have four nested domains with horizontal resolutions of 54, 18, 6, and 2 km, respectively. The initial vortex has a maximum wind speed (Vmax) of 25 m s^{-1} at a radius of 100 km near the surface, and then decreases with height. The details on the model configuration can be referred to in Ge (2015). In the control experiment (CTL), the Jordan (1958) sounding is applied to represent the summer mean condition of the Caribbean. In the sensitivity experiment, the temperature profile is modified to mimic a warmer environment. The model strategy follows Stovern and Ritchie (2016), in which the importance of the ambient temperature profile on TC size and structure was investigated. That is, in a warmer environment (WARM), the temperature is uniformly increased by 1.5°C in all the vertical levels compared to CTL. By doing so, the static stability is enhanced in WARM. To maintain a consistent moisture profile with the increased temperatures, the specific humidity is increased to maintain a constant relative humidity. Both vortices are spun up on an f-plane (centered at 15°N) in a quiescent environment with a constant SST of 29°C.

To investigate the possible impacts of the moist entropy within the moat region on the demise of the inner eyewall, two additional sensitivity experiments are conducted, in which the surface fluxes within moat region are artificially changed. Specifically, the surface heat fluxes within the moat region are increased (reduced) by 50% in SFL_1.5 (SFL_0.5), respectively. More details on these experiments will be further introduced in section 4. In the current study, we mainly focus on the different evolutions of the secondary eyewalls in the simulations. In particular, the possible mechanisms by which the structure of the secondary eyewall affects the duration of the ERC are examined.

3. Simulated SEF

Figure 1 shows that, in both CTL and WARM, the storm evolves into a configuration where a secondary wind maximum is evident at a certain radius. In the current study, ERC onset is defined as the time when there is a secondary maximum tangential wind and enhanced radar reflectivity. ERC completion is defined as the time of inner-eyewall demise. Notice that there are salient differences in the timing of SEF. Specifically, SEF occurs after around 105 (162) hours of simulation in CTL (WARM). These results indicate that the timing of the onset of the secondary eyewall is sensitive to the environmental conditions. In addition to the timing of SEF, the storm intensity and structure show marked discrepancies. Specifically, the secondary eyewall emanates at a radius of 90 km in CTL, whereas it is located at around 125 km in WARM. As a result, the moat width is larger in WARM than in CTL.

Generally, both cases bear many similarities to the canonical ERC (i.e., Willoughby et al., 1984; Houze et al., 2007). That is, TC intensity initially weakens and then re-intensifies during the ERC. Nevertheless, the intensity fluctuations show significant differences. Prior to SEF, both cases have similar Vmax (approximately 70 m s^{-1}). In CTL, the Vmax initially reduces to 50 m s^{-1} when the inner eyewall decays, but then recovers to 70 m s^{-1} after ERC completion. In contrast, in WARM, the Vmax initially weakens to 50 m s^{-1}, but only re-intensifies to 60 m s^{-1} after the ERC. Furthermore, the separation between the inner and outer radius of maximum wind (RMW) is about 60 and 85 km in CTL and WARM, respectively. Given the different characteristics of intensity change and structure, we suggest that the intensity changes are closely related to the structure of the secondary eyewall during the ERC. Under the conditions of WARM, a TC with a larger moat width will experience a greater weakening of intensity, which supports the findings of previous studies (Zhou and Wang, 2011, 2013; Ge, 2015).

In short, the simulated ERC is highly sensitive to the ambient thermal conditions. In a warmer atmosphere with enhanced static stability, SEF is much delayed, and the outer eyewall occurs at a larger outer radius and thus a wider moat area. Furthermore, the TC with a wider moat tends to experience a prolonged ERC. Next, we attempt to elucidate the

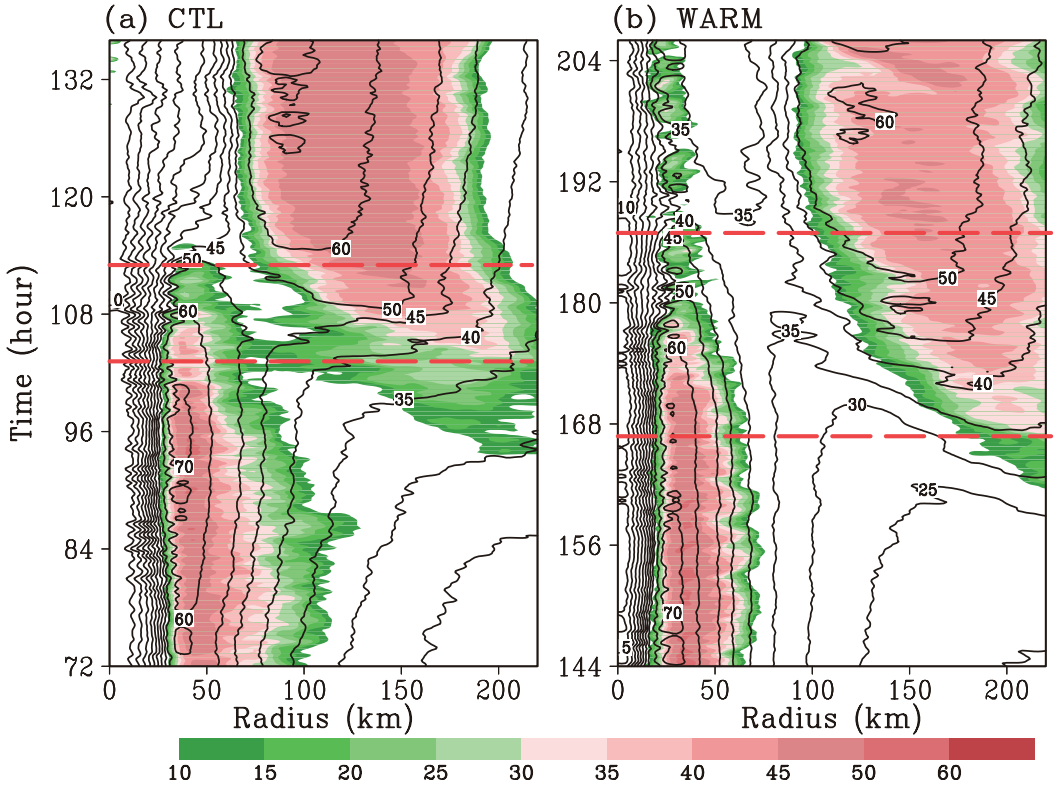

Fig. 1. Radius–time cross sections of the azimuthal-mean tangential wind velocity (contours; units: m s^{-1}) and radar reflectivity (shaded; units: dBZ) at the height of 2 km in (a) CTL and (b) WARM. The red lines denote the period of the ERC.

possible underlying physical processes.

4. Physical interpretation

4.1. *Onset of SEF*

The results indicate that SEF is much delayed in WARM, with an enhanced static stability. The warming, while maintaining consistent relative humidity, results in higher specific humidity and smaller moisture fluxes from the ocean. As such, the enhanced static stability greatly suppresses outer-core convection and thus yields slow intensification and a smaller outer size (Stovern and Ritchie, 2016). Ge et al. (2016) found that the timing of SEF is very sensitive to the initial TC outer size (i.e., the radius of 34-knots wind; R34). A larger outer size tends to promote rapid SEF. The simulations here show that SEF occurs much earlier in CTL than in WARM. The results agree well with previous studies (Ge et al., 2016; Stovern and Ritchie, 2016).

Furthermore, the idea of unbalanced dynamics in the boundary layer has also been proposed (Huang et al., 2012; Abarca and Montgomery, 2013). In this paradigm, the unbalanced response in the boundary layer acts as an important mechanism for SEF. This hypothesis emphasizes that a broadening of the tangential wind, with enhanced supergradient winds in the boundary layer, forces convection outside of the primary eyewall, leading to SEF. The agradient wind force (AF) in the boundary layer is measured by the differences among the centrifugal force, Coriolis force, and the local radial pressure gradient. Specifically, a negative (positive) AF means a subgradient (supergradient) wind force, and thus indicates a tendency to enhance the inflows towards (outflow away from) the vortex center. Figure 2, which compares the boundary layer imbalances in CTL and WARM, shows that the patterns are generally quite similar to the radar reflectivity, since the enhanced convection is associated with considerable boundary layer imbalances. In CTL, the radially outward AF (positive value) emanates and occurs mainly at $100 < r < 130$ km. For WARM, the radial location of the supergradient zone is mainly confined to around $125 < r < 175$ km, which is farther away from the center than that in CTL. In the SEF region, the positive AF strengthens with time. The enhancement of supergradient winds leads to a rapidly decelerating radial inflow. As such, this leads to a region of convergence and thus an eruption of deep convection therein (not shown). The result is consistent with Huang et al. (2012). Moreover, the strong positive AF emanates earlier in CTL, and its radial location is closer to the center. In contrast, the positive AF is much more delayed and located at a larger radius in WARM. By this reasoning, the time sequences of the boundary layer imbalances can reasonably explain the difference in SEF.

Close examination also shows that, prior to SEF, it is evident that the enhanced tangential winds within the boundary

layer occur in the outer region. As pointed out by Rozoff et al. (2012), along with the expanding swirling wind, the elevated inertial stability will favor the intensification of outer convection, since axisymmetric efficiency is related to the inertial parameter. In this regard, Fig. 3 compares the temporal evolution of the diabatic heating and kinetic energy averaged over the ring where the outer eyewall is located. That is, it is averaged over radii of 100–125 km and 125–150 km in

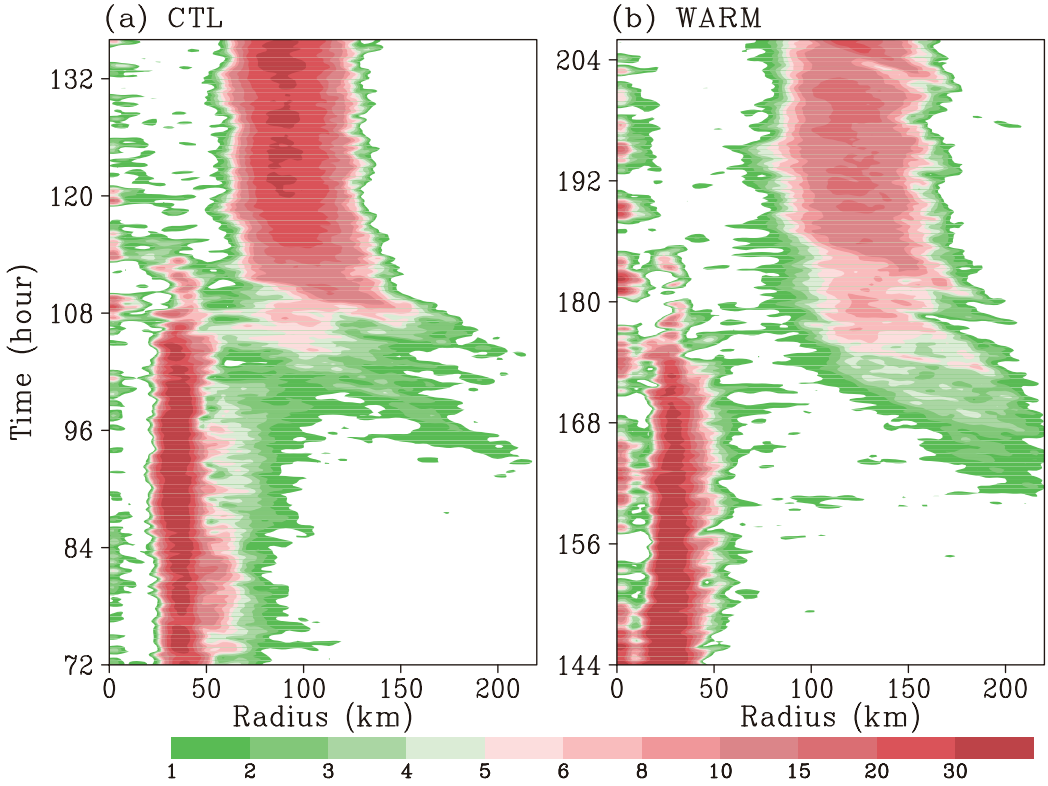

Fig. 2. Radial–time cross sections of the boundary layer imbalances at the height 1 km in (a) CTL and (b) WARM. Positive AF (units: m s^{-1} h^{-1}) is shaded.

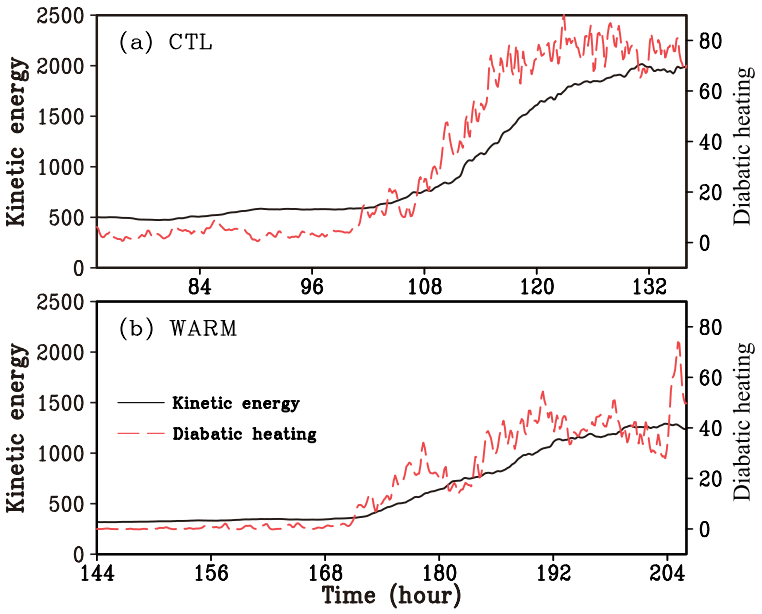

Fig. 3. Temporal evolution of the diabatic heating (units: K s^{-1}) and kinetic energy (units: m^2 s^{-2}) averaged over the radius where the outer eyewall is located in (a) CTL and (b) WARM.

CTL and WARM, respectively. As expected, there is an obvious relationship between the averaged diabatic heating and kinetic energy. Along with the onset of SEF, both variables are greatly enhanced with time. It is anticipated that an expansive wind field leads to a higher inertial stability, which will readily help the conversion of latent heating to kinetic energy (Schubert and Hack, 1982; Hack and Schubert, 1986; Rozoff et al., 2012).

4.2. *Duration of the ERC*

Previous numerical simulations (Terwey and Montgomery, 2008; Zhou and Wang, 2009) have shown that the simulated ERC duration generally falls within a range of 6–18 h, indicating it is variable. Hence, it is vital to understand the processes affecting ERC duration.

Here, we attempt to answer the following question: what determines the timing of the demise of the inner eyewall and the completion of an ERC? A number of possible mechanisms have been proposed in previous studies (Rozoff et al., 2008), including: (1) the development of an outer eyewall that effectively chokes the inner eyewall convection by intercepting the boundary layer supply of moist entropy; (2) the possible weakening of inner eyewall convection by subsidence forced by the outer eyewall; (3) the suppression of inner-area convection by enhanced static stability associated with the warm core; and (4) the wave dynamics and mixing process associated with barotropic instability (Kossin et al., 2000; Hendricks et al., 2014). We focus on these mechanisms in the following part of our study.

First, the choking effect is investigated by comparing the evolution of low-level radial inflows in both cases (Fig. 4). It is apparent that, once the secondary eyewall is formed, the maximum radial inflows shift to the outside of the outer eyewall. Notice that the low-level inflows are much stronger in CTL than in WARM. It is likely that, as the secondary eyewall is established, the boundary layer supergradient force is enhanced (Fig. 2), leading to a rapidly decelerating radial inflow towards the original inner-eyewall region. Compared with CTL, the AF is much smaller and thus the deceleration of inflow towards the inner eyewall is slower in WARM.

To examine the mechanism for primary eyewall demise, the vertical–radial cross sections of equivalent potential temperatures (θ_e) during the ERC are compared (Fig. 5). As we can see, θ_e decreases with the radius, and has a greater radial gradient in the regions of the eyewall. A relatively weaker radial gradient of θ_e exists in the moat region. Interestingly, the radial gradient of θ_e within the moat region is much weaker in WARM. It has been pointed out that the supply of moist entropy is closely related to the mean horizontal advection (Zhou and Wang, 2011). Therefore, the mean horizontal advection of θ_e within moat region is specifically compared (Fig. 6). The horizontal advection term is negative and more significant in CTL than WARM. By this reasoning, the greater negative effect may quickly reduce the moist entropy supply in the inner-eyewall region, and thus accelerates the decaying of the inner eyewall. As such, the choking effect seems to play a certain role in the demise of the inner eyewall

To further confirm the possible impacts of the moist entropy within the moat region, two sensitivity experiments are conducted. It is known that boundary layer moist entropy is associated with the surface heat fluxes (Bryan and Rotunno, 2009). Hence, two additional sensitivity experiments are

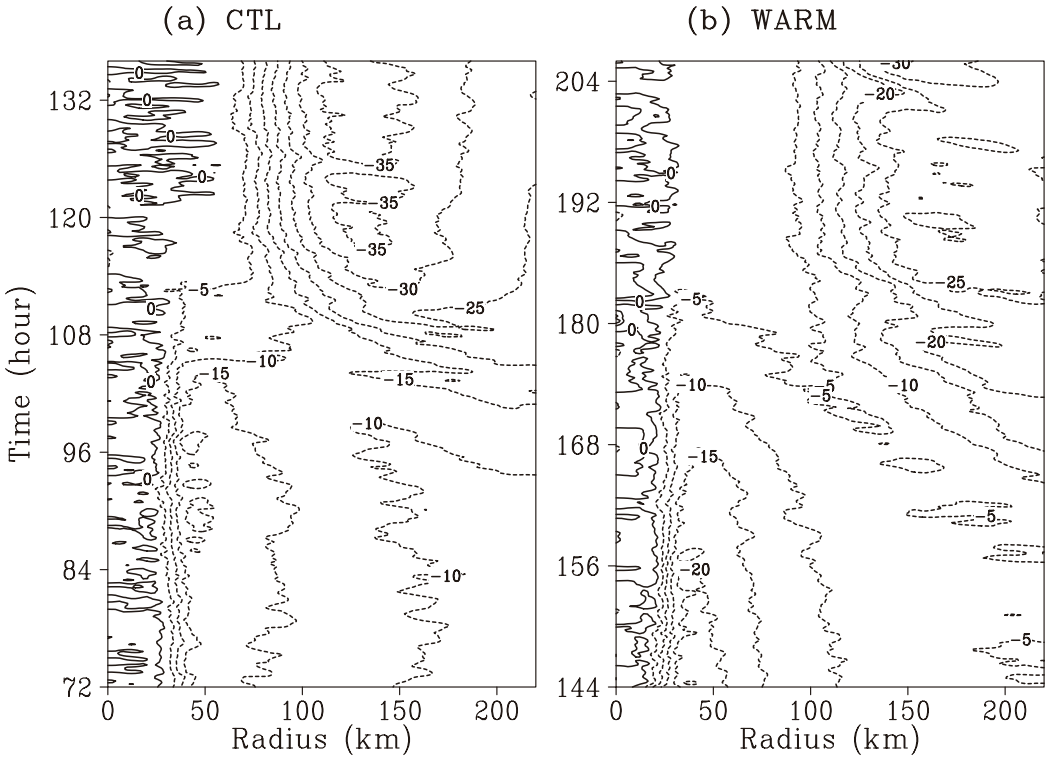

Fig. 4. Radial–time cross section of radial inflow (units: m s^{-1}) at the height of 1 km in (a) CTL and (b) WARM.

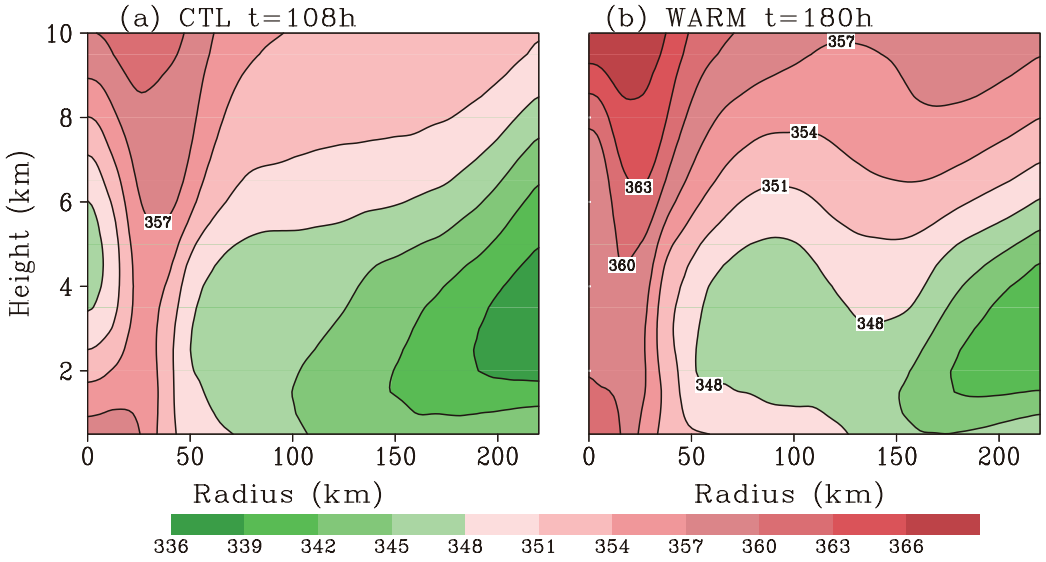

Fig. 5. Vertical–radial cross section of equivalent potential temperature (units: K) during the ERC in (a) CTL and (b) WARM.

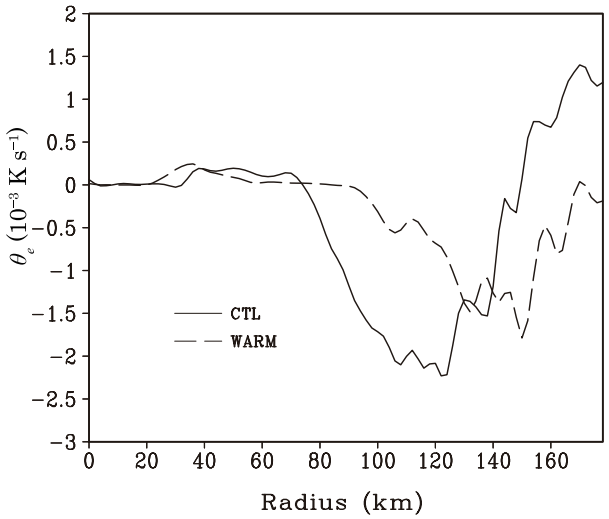

Fig. 6. Horizontal advection of θ_e (units: 10^{-3} K s^{-1}) during the ERC in the two simulations.

designed to artificially change the surface fluxes. The model output from WARM at t = 162 h is chosen as the restarting point, and then continues to integrate for 36 h. Specifically, while calculating the surface heat fluxes, the simulated 10-m wind speed within a radius of 75–125 km is increased (reduced) 50% in SFL_1.5 (SFL_0.5), respectively. This artificially alters the surface fluxes at the specific radius.

Figure 7 shows the evolution of azimuthal mean tangential winds and radar reflectivity in SFL_1.5 and SFL_0.5, separately. Of particular interest is that the duration of the ERC shows a salient difference. That is, the inner eyewall maintains for a longer time in SFL_1.5 than in SFL_0.5. The results clearly suggest that the moist entropy within the moat region likely affects the inner-eyewall convection. Close examination shows that, in SFL_1.5, the moist entropy in the boundary layer is enhanced due to the enhanced surface fluxes (not shown).

Secondly, the hypothesis that the subsidence forced by the outer eyewall likely weakens the inner-eyewall convection is investigated. For this purpose, the Sawyer–Eliassen (SE) balance equation (Schubert and Hack, 1982; Willoughby, 2009) is applied. This method has been extensively used to diagnose the adjustment to a quasi-balanced state. In the present study, the azimuthal mean diabatic heating forcing associated with the outer eyewall is only considered. Figure 8 compares the vertical motion forced by diabatic heating associated with outer-eyewall convection in CTL and WARM, separately. It is evident that, adjacent to the heating source, the forced descending motion is much stronger in CTL. Physically, for a typical TC, the smaller the radius, the larger the inertial stability. The larger inertial parameter tends to limit the horizontal extension, thus favoring an enhanced vertical motion. The radial location of the maximum diabatic heating of the outer eyewall in CTL is closer to the TC center. As a result, strong descending motion within the inner-core area is unfavorable for inner-eyewall convection. The results suggest that the magnitude and radial location of outer-eyewall convection are possible key factors influencing the decay of the inner eyewall.

Thirdly, the static stability in the inner-core area during the ERC is compared. It is speculated that, during the ERC, the warm core extends and takes over the moat region. Figure 9 compares the vertical–radial cross sections of the warm core between CTL and WARM. Evidently, the warm core is significantly pronounced in CTL, especially at the middle levels (6–8 km), implying a pronounced static stability therein. Although the initial ambient static stability is larger in WARM, it becomes greater in the inner core in CTL. This is partly due to the different descending motion forced by the outer eyewall, as shown in Fig. 8. That is, in CTL, a stronger

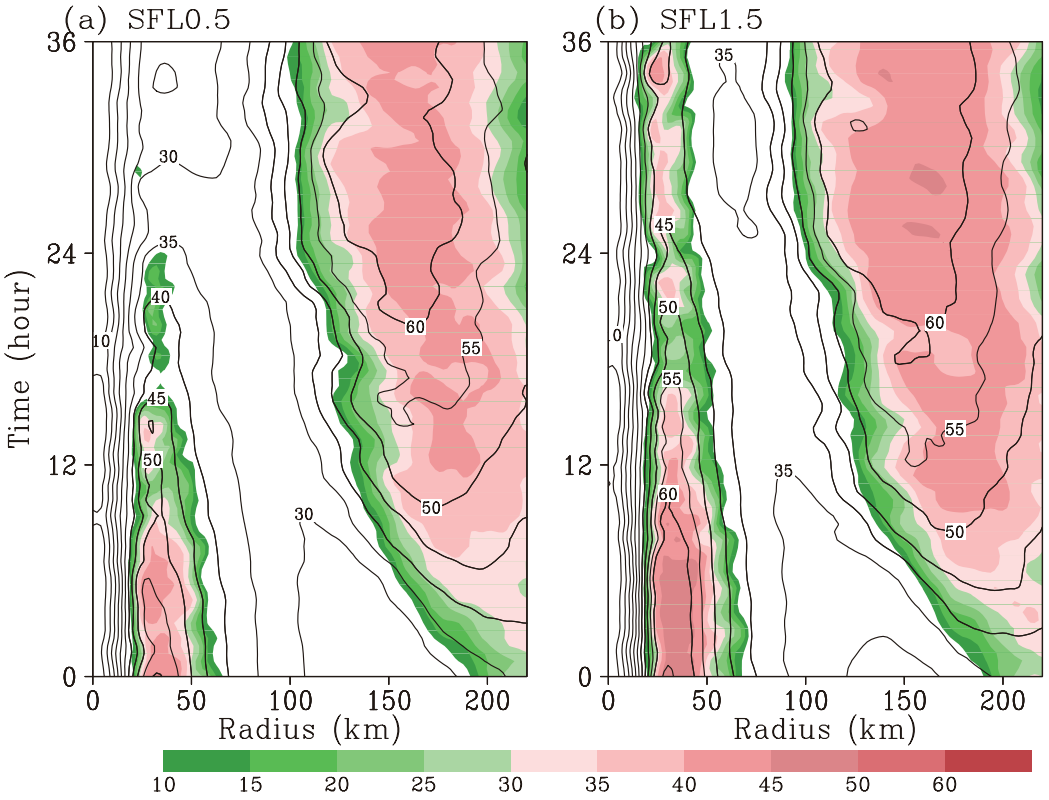

Fig. 7. Evolution of azimuthal-mean tangential wind (contours; units: m s^{-1}) and radar reflectivity (shaded; units: dBZ) in (a) SFL_0.5 and (b) SFL_1.5.

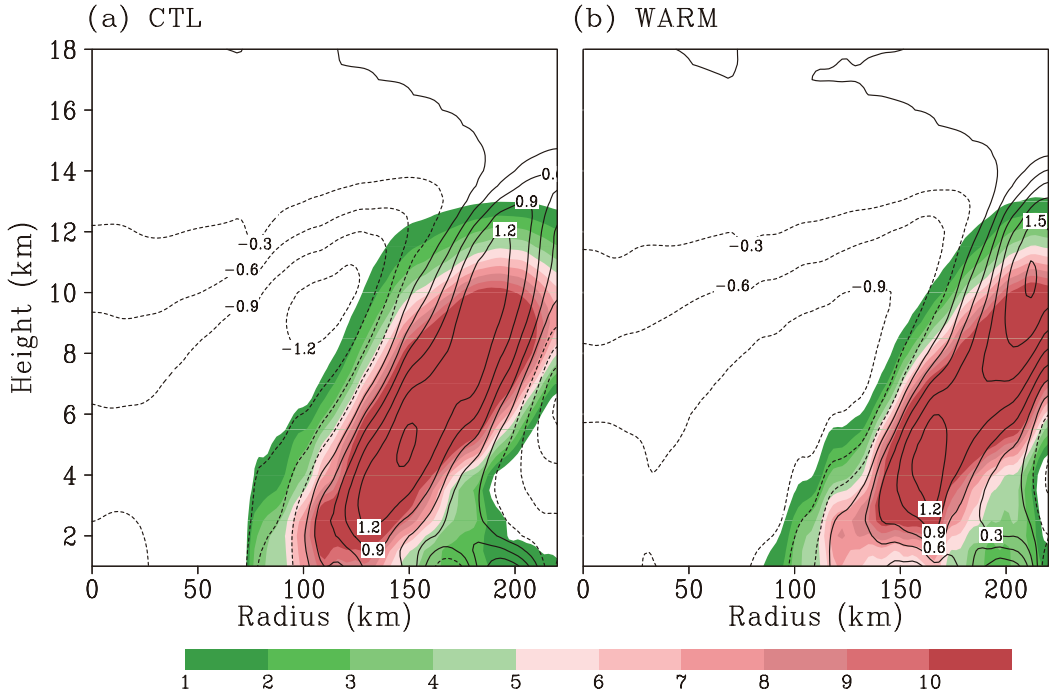

Fig. 8. Vertical velocity (contours; units: m s^{-1}) forced by diabatic heating (shaded; units: K s^{-1}) associated with the outer eyewall through the SE equation in (a) CTL and (b) WARM.

inner-core descending motion is conducive to rapidly rebuilding the warm core, which promotes static stability and is thus unfavorable for inner-eyewall convection. Since a wider moat reflects a wider warm core after the ERC, it generally takes a longer time to rebuild the warm core. In this regard, a smaller moat region implies a quicker establishment of the

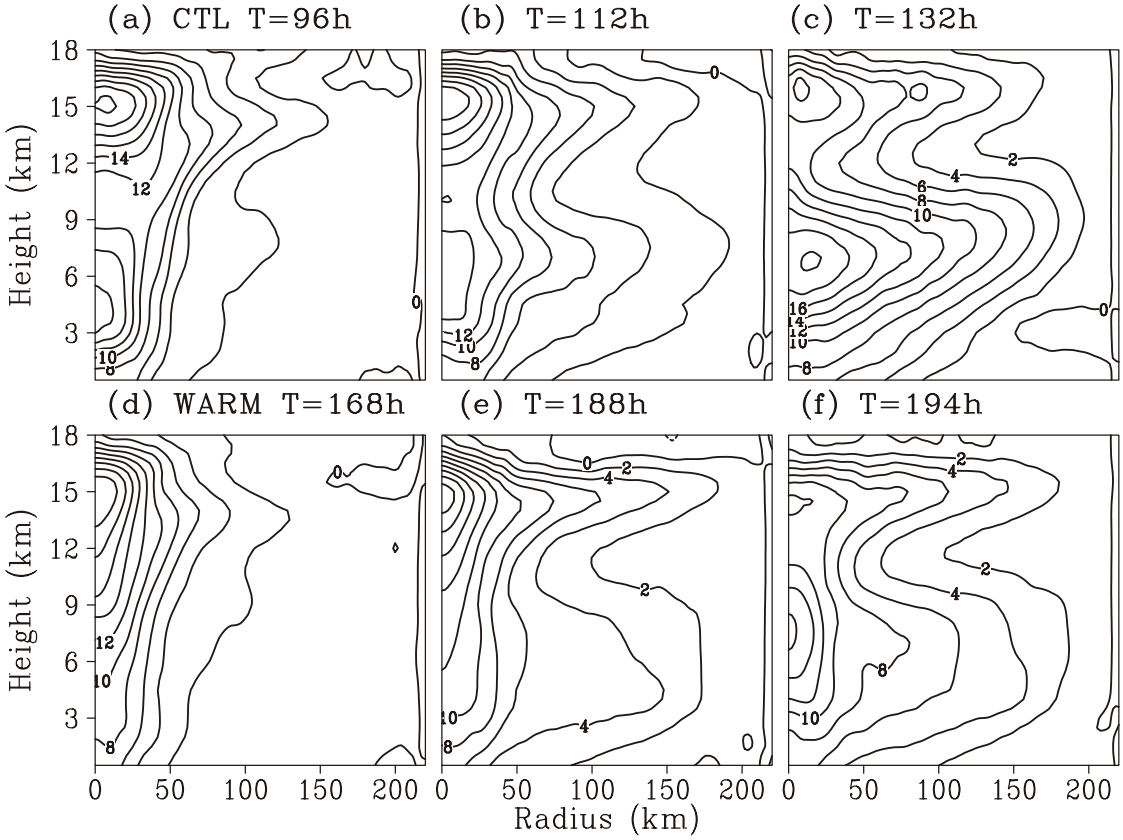

Fig. 9. Snapshots of the vertical–radius cross section of the warm core (units: K) during the ERC in (a–c) CTL and (d–f) WARM.

warm core in CTL, which reasonably accounts for the TC intensity change during the ERC.

Lastly, the process associated with barotropic instability is examined. For a typical TC with a concentric eyewall structure, the relative vorticity field shows a ring-like structure in both eyewall regions. The sign reversal of the radial gradient of vorticity in the inner and outer eyewall satisfies the necessary condition for barotropic instability (Kossin and Sitkowski, 2009). The counter-propagating VRWs associated with the inner and outer eyewall may interact, leading to wave breaking and thus mixing. To address this possibility, we attempt to explore the interaction using the model output. The Eliassen–Palm (EP) flux has been widely used to diagnose the wave energy propagation and wave-mean flow interaction (Molinari et al., 1995; Chen et al., 2003). Provided that the wave-mean flow interaction is proportional to its EP flux divergence, it is useful to compare the EP flux divergence term in CTL and WARM.

The EP flux divergence in an isentropic vertical coordinate is formulated as

$$\nabla \cdot \boldsymbol{F} = -\frac{1}{r}\frac{\partial}{\partial r} r^2 \overline{(\sigma u_L)' v_L'} + \frac{\partial}{\partial \theta} \overline{p' \frac{\partial \Psi'}{\partial \lambda}} \,,$$

where

$$\boldsymbol{F} \equiv \left\{ -r\overline{(\sigma u_L)' v_L'}, \overline{p'[\partial \Psi'/(\partial \lambda)]} \right\} \,,$$

is the EP flux vector, which is calculated on cylindrical coordinates, the overbar represents the azimuthal mean, and the prime is the deviation from the mean. Here, u_L' and v_L' are the storm-relative radial and tangential winds, respectively; λ is the azimuthal angle; $\sigma = -\partial p/\partial \theta$ is the pseudodensity; r is the radius; p is the pressure; θ is the potential temperature; and Ψ' is the Montgomery streamfunction. Figure 10 shows the vertical–radius cross section of the EP flux divergence and symmetric component of tangential wind. It clearly shows that, within the moat region, the magnitude of the divergence term is greater in CTL than in WARM, implying a greater interaction in the former. Meanwhile, a negative divergence term coincides with the RMW, and positive values exist to both sides. Physically, a negative (positive) EP flux divergence term weakens (enhances) the mean flow. This suggests that eddies tend to counteract the mean circulation at the RMW, but accelerate the winds both sides of the RMW. This is consistent with Chen et al. (2003). In short, while this method can compare the importance of wave-mean interaction during the ERC, the detailed wave properties, such as VRWs, cannot be explored. As such, more analyses are needed to reveal the underlying physical processes.

5. Conclusion and discussion

In this study, the impacts of ambient temperature on the ERC in TCs are examined using idealized numerical simulations. The results show that the duration of the ERC and the associated intensity change are sensitive to the ambient

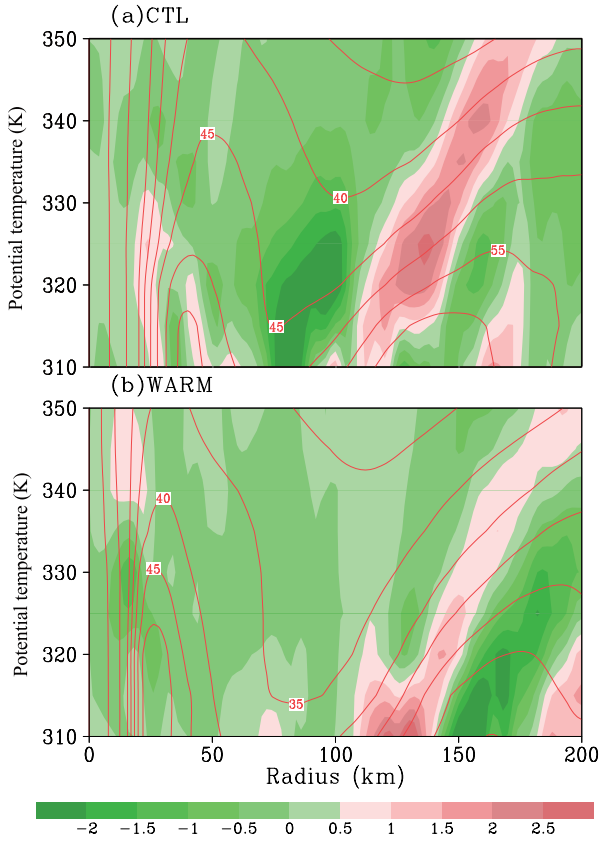

Fig. 10. Vertical–radius cross section of the EP flux divergence (shaded; units: 10^{-3} m s^{-2}) and azimuthal-mean tangential wind (contours; units: m s^{-1}) in (a) CTL and (b) WARM.

temperature profile. It is revealed that enhanced static stability will greatly suppress convection and thus slow intensification and reduce the outer size. The timing of SEF is sensitive to the outer size of the TC. In short, we find that the simulated ERC is highly sensitive to the ambient thermal conditions. In a warmer atmosphere with enhanced static stability, SEF is much delayed, and the outer eyewall occurs at a larger outer radius and thus a wider moat area. Furthermore, a TC with a wider moat tends to experience a prolonged ERC.

The processes that lead to the TC intensity and structural changes are investigated. It is found that the choking effect and the distribution of moist entropy within the moat region likely impact the inner-eyewall convection. Consistent with Zhou and Wang (2011), the negative mean horizontal advection of moisture entropy helps the decay of the inner eyewall. Meanwhile, the radial distribution of outer heating probably influences inner-eyewall convection through forced descending motion. As the inner eyewall decays, the warm core extends and takes over the moat region. Accompanied by the rebuilding of the warm core, the inner-core static stability changes accordingly, which affects the inner-eyewall convection. EP flux analysis shows that the interaction between the inner and outer eyewall, due to the barotropic instability, is also sensitive to their radial separation. It is speculated that a larger radial separation results in a weaker interaction between the inner and outer eyewall, and thus slows down the wave-breaking and mixing process.

Although these processes contribute to the behavior of the ERC, their relative roles are not clear. Moreover, the analyses in this study are only based on a set of idealized numerical simulations without environmental flows. It is anticipated that different environmental flows may introduce different forcing that affects the deep convection, thus limiting the potential for SEF and affecting its structure. The external forcing affects TC structure and intensity changes either directly or indirectly through the mesoscale processes in both the inner-core region and outer spiral rainbands, which affect SEF and the subsequent eyewall replacement. Therefore, more complicated environmental flows should be considered in future work. This study provides strong motivation for further investigations into how environmental conditions influence TC dynamics and thermodynamics.

Acknowledgements. This work was jointly sponsored by the National Science Foundation of China (Grant No. 41575056), the National Key Basic Research Program of China (Grant No. 2015CB452803), the Special Fund Project for Meteorology Research in the Public Interest (Grant No. 201506007), the Key Technology Integration and Application Project of the China Meteorological Administration, and the Priority Academic Program Development of Jiangsu Higher Education Institutions.

REFERENCES

Abarca, S. F., and M. T. Montgomery, 2013: Essential dynamics of secondary eyewall formation. *J. Atmos. Sci.*, **70**, 3216–3230, doi: 10.1175/JAS-D-12-0318.1.

Bell, M. M., M. T. Montgomery, and W.-C. Lee, 2012: An axisymmetric view of concentric eyewall evolution in Hurricane Rita (2005). *J. Atmos. Sci.*, **69**, 2414–2432, doi: 10.1175/JAS-D-11-0167.1.

Black, M. L., and H. E. Willoughby, 1992: The concentric eyewall cycle of Hurricane Gilbert. *Mon. Wea. Rev.*, **120**, 947–957, doi: 10.1175/1520-0493(1992)120<0947:TCECOH>2.0.CO;2.

Bryan, G. H., and R. Rotunno, 2009: The maximum intensity of tropical cyclones in axisymmetric numerical model simulations. *Mon. Wea. Rev.*, **137**, 1770–1789, doi: 10.1175/2008MWR2709.1.

Chen, Y. S., G. Brunet, and M. K. Yau, 2003: Spiral bands in a simulated hurricane. Part II: Wave activity diagnostics. *J. Atmos. Sci.*, **60**, 1239–1256, doi: 10.1175/1520-0469(2003)60<1239:SBIASH>2.0.CO;2.

Ge, X. Y., 2015: Impacts of environmental humidity on concentric eyewall structure. *Atmos. Sci. Letts.*, **16**, 273–278, doi: 10.1002/asl2.553.

Ge, X. Y., L. Guan, and S. W. Zhou, 2016: Impacts of initial structure of tropical cyclone on secondary eyewall formation. *Atmos. Sci. Lett.*, **17**, 569–574, doi: 10.1002/asl.707.

Hack, J. J., and W. H. Schubert, 1986: Nonlinear response of atmospheric vortices to heating by organized cumulus convection. *J. Atmos. Sci.*, **43**, 1559–1573, doi: 10.1175/1520-0469(1986)043<1559:NROAVT>2.0.CO;2.

Hawkins, J. D., M. Helveston, T. F. Lee, J. F. Turk, K. Richard-

son, C. Sampson, J. Kent, and R. Wade, 2006: Tropical cyclone multiple eyewall configurations. *Preprints*, *27th Conference on Hurricanes and Tropical Meteorology*, Amer. Meteor. Soc., Monterey, CA,

Hendricks, E. A., W. H. Schubert, Y. H. Chen, H. C. Kuo, and M. S. Peng, 2014: Hurricane eyewall evolution in a forced shallow-water model. *J. Atmos. Sci*., **71**, 1623–1643, doi: 10.1175/JAS-D-13-0303.1.

Houze, R. A., Jr., S. S. Chen, B. F. Smull, W.-C. Lee, and M. M. Bell, 2007: Hurricane intensity and eyewall replacement. *Science*, **315**, 1235–1239, doi: 10.1126/science.1135650.

Huang, Y.-H., M. T. Montgomery, and C.-C. Wu, 2012: Concentric eyewall formation in Typhoon Sinlaku (2008). Part II: Axisymmetric dynamical processes. *J. Atmos. Sci*., **69**, 662–674, doi: 10.1175/JAS-D-11-0114.1.

Jordan, C. L., 1958: Mean soundings for the West Indies area. *J. Atmos. Sci*., **15**, 91–97, doi: 10.1175/1520-0469(1958)015<0091:MSFTWI>2.0.CO;2.

Judt, F., and S. S. Chen, 2010: Convectively generated potential vorticity in rainbands and formation of the secondary eyewall in Hurricane Rita of 2005. *J. Atmos. Sci.*, **67**, 3581–3599, doi: 10.1175/2010JAS3471.1.

Kossin, J. P., and M. Sitkowski, 2009: An objective model for identifying secondary eyewall formation in hurricanes. *Mon. Wea. Rev*., **137**, 876–892, doi: 10.1175/2008MWR2701.1.

Kossin, J. P., W. H. Schubert, and M. T. Montgomery, 2000: Unstable interactions between a hurricane's primary eyewall and a secondary ring of enhanced vorticity. *J. Atmos. Sci.*, **57**, 3893–3917, doi: 10.1175/1520-0469(2001)058<3893:UIBAHS>2.0.CO;2.

Kuo, H.-C., L.-Y. Lin, C.-P. Chang, and R. T. Williams, 2004: The formation of concentric vorticity structures in typhoons. *J. Atmos. Sci*., **61**, 2722–2734, doi: 10.1175/JAS3286.1.

Kuo, H.-C., W. H. Schubert, C.-L. Tsai, and Y.-F. Kuo, 2008: Vortex interactions and barotropic aspects of concentric eyewall formation. *Mon. Wea. Rev*., **136**, 5183–5198, doi: 10.1175/2008MWR2378.1.

Molinari, J., S. Skubis, and D. Vollaro, 1995: External influences on hurricane intensity. Part III: Potential vorticity structure. *J. Atmos. Sci.*, **52**, 3593–3606, doi: 10.1175/1520-0469(1995)052<3593:EIOHIP>2.0.CO;2.

Montgomery, M. T., and R. J. Kallenbach, 1997: A theory for vortex Rossby-waves and its application to spiral bands and intensity changes in hurricanes. *Quart. J. Roy. Meteor. Soc*., **123**, 435–465, doi: 10.1002/qj.49712353810.

Nong, S. Y., and K. Emanuel, 2003: A numerical study of the genesis of concentric eyewalls in hurricanes. *Quart. J. Roy. Meteor. Soc*., **129**, 3323–3338, doi: 10.1256/qj.01.132.

Qiu, X., and Z.-M. Tan, 2013: The roles of asymmetric inflow forcing induced by outer rainbands in tropical cyclone secondary eyewall formation. *J. Atmos. Sci.*, **70**, 953–974, doi: 10.1175/JAS-D-12-084.1.

Qiu, X., Z. M. Tan, and Q. N. Xiao, 2010: The roles of vortex Rossby waves in hurricane secondary eyewall formation. *Mon. Wea. Rev*., **138**, 2092–2109, doi: 10.1175/2010MWR3161.1.

Rozoff, C. M., W. H. Schubert, B. D. McNoldy, and J. P. Kossin, 2006: Rapid filamentation zones in intense tropical cyclones. *J. Atmos. Sci*., **63**, 325–340, doi: 10.1175/JAS3595.1.

Rozoff, C. M., W. H. Schubert, and J. P. Kossin, 2008: Some dynamical aspects of tropical cyclone concentric eyewalls. *Quart. J. Roy. Meteor. Soc*., **134**, 583–593, doi: 10.1002/qj.237.

Rozoff, C. M., D. S. Nolan, J. P. Kossin, F. Q. Zhang, and J. Fang, 2012: The roles of an expanding wind field and inertial stability in tropical cyclone secondary eyewall formation. *J. Atmos. Sci.*, **69**, 2621–2643, doi: 10.1175/JAS-D-11-0326.1.

Schubert, W. H., and J. J. Hack, 1982: Inertial stability and tropical cyclone development. *J. Atmos. Sci.*, **39**, 1687–1697, doi: 10.1175/1520-0469(1982)039<1687:ISATCD>2.0.CO;2.

Stovern, D. R., and E. A. Ritchie, 2016: Simulated sensitivity of tropical cyclone size and structure to the atmospheric temperature profile. *J. Atmos. Sci.*, **71**, 4553–4571, doi: 10.1175/JAS-D-15-0186.1.

Terwey, W. D., and M. T. Montgomery, 2008: Secondary eyewall formation in two idealized, full-physics modeled hurricanes. *J. Geophys. Res*., **113**(D12), D12112, doi: 10.1029/2007JD008897.

Willoughby, H. E., 2009: Diabatically induced secondary flows in tropical cyclones. Part II: Periodic forcing. *Mon. Wea. Rev*., **137**, 822–835, doi: 10.1175/2008MWR2658.1.

Willoughby, H. E., J. A. Clos, and M. G. Shoreibah, 1982: Concentric eye walls, secondary wind maxima, and the evolution of the hurricane vortex. *J. Atmos. Sci.*, **39**, 395–411, doi: 10.1175/1520-0469(1982)039<0395:CEWSWM>2.0.CO;2.

Willoughby, H. E., H.-L. Jin, S. J. Lord, and J. M. Piotrowicz, 1984: Hurricane structure and evolution as simulated by an axisymmetric, nonhydrostatic numerical model. *J. Atmos. Sci.*, **41**, 1169–1186, doi: 10.1175/1520-0469(1984)041<1169:HSAEAS>2.0.CO;2.

Yang, Y. T., H. C. Kuo, E. A. Hendricks, and M. S. Peng, 2013: Structural and intensity changes of concentric eyewall typhoons in the western north pacific basin. *Mon. Wea. Rev*., **141**, 2632–2648, doi: 10.1175/MWR-D-12-00251.1.

Zhang, F. Q., D. D. Tao, Y. Q. Sun, and J. D. Kepert, 2017: Dynamics and predictability of secondary eyewall formation in sheared tropical cyclones. *Journal of Advances in Modeling Earth Systems*, doi: 10.1002/2016MS000729.

Zhou, X. Q., and B. Wang, 2009: From concentric eyewall to annular hurricane: A numerical study with the cloud-resolved WRF model. *Geophys. Res. Lett*., **36**, L03802, doi: 10.1029/2008GL036854.

Zhou, X. Q., and B. Wang, 2011: Mechanism of Concentric eyewall replacement cycles and associated intensity change. *J. Atmos. Sci.*, **68**, 972–988, doi: 10.1175/2011JAS3575.1.

Zhou, X. Q., and B. Wang, 2013: Large-scale influences on secondary eyewall size. *J. Geophys. Res*., **118**, 11 088–11 097, doi: 10.1002/jgrd.50605.

Zhu, P., and Coauthors, 2015: Impact of subgrid-scale processes on eyewall replacement cycle of tropical cyclones in HWRF system. *Geophys. Res. Lett*., **42**, 10 027–10 036, doi: 10.1002/2015GL066436.

Zhu, Z.-D., and P. Zhu, 2014: The role of outer rainband convection in governing the eyewall replacement cycle in numerical simulations of tropical cyclones, *J. Geophys. Res*., **119**, 8049–8072, doi: 10.1002/2014JD021899.

Zhu, Z. D., and P. Zhu, 2015: Sensitivities of eyewall replacement cycle to model physics, vortex structure, and background winds in numerical simulations of tropical cyclones. *J. Geophys. Res*., **102**, 590–622, doi: 10.1002/2014JD022056.